




Two-mode Raman quantum battery dependent on coupling strengthLu Wang,¹ Shu-Qian Liu,¹ Feng-lin Wu,^{1,2} Hao Fan ¹ and Si-Yuan Liu ^{1,2,*}¹*Institute of Modern Physics, Northwest University, Xi'an 710127, China*²*Shaanxi Key Laboratory for Theoretical Physics Frontiers, Xi'an 710127, China* (Received 10 July 2023; revised 20 August 2023; accepted 9 November 2023; published 4 December 2023)

We investigate a series of two-mode quantum batteries (QBs) which exhibits better performance in both the stored energy and average charging power compared to the two-photon case. In both the model related to coupling strength and Raman cases, we find the QBs can store energy faster and have a higher efficiency than the original case. Among the derived models we have studied, the two-mode Raman QB dependent on coupling strength has the best performance. We also present the relationship between the ergotropy and battery-charger entanglement of incoherent QBs and define the resource utilization efficiency $k(t)$ and $k^{\text{ins}}(t)$. We find that entanglement in the energy-extraction stage is a key resource. In addition, we consider a collection of two-level systems embedded in a two-mode microwave cavity with counterrotating terms, which shows that the counterrotating terms lead to a higher stored energy in the ultrastrong-coupling regime.

DOI: [10.1103/PhysRevA.108.062402](https://doi.org/10.1103/PhysRevA.108.062402)**I. INTRODUCTION**

With the continuous development of quantum technology [1–3], it has been possible to access and manipulate microscopic systems with very high precision at the level of a single atom or single photon. Quantum resources, such as coherence and entanglement, play a crucial role from both theoretical and applied perspectives. Researchers are also working on using quantum resources to bypass bottlenecks in classical physics and improving computing power and device performance [4]. With this background, Alicki and Fannes first proposed the concept of quantum battery [5]. They tried to use nonclassical effects to give quantum batteries (QBs) more advantages than classical batteries, such as shorter charging time and higher charging efficiency [6–11].

Theoretical schemes for possible QBs are usually based on two-level systems (TLSs), such as trapped ions [12–14], superconducting qubits [15], and quantum dots in semiconductors [16]. These platforms can be used as batteries and coupled to chargers with different properties that can coherently transfer energy to them. One of the most important charging schemes is energy transformed from a microwave cavity [17–20] to a series of interacting TLSs [21–23]. For such a QB, it is shown that the average charging power can be increased by the collective interactions between the N TLSs. Specifically, the scale of this enhancement is proportional to the square root of the number of TLSs involved, denoted as \sqrt{N} [8,24,25]. Interestingly, a similar scale which is in agreement with theoretical predictions was reported in a recent experiment for the first time [26].

In addition, recent theoretical studies showed that the two-mode cavity model [27–29] is similar to the two-photon model [30,31]. Both of them can be implemented through circuit

electrodynamics. And they can characterize the process of a TLS transition with the absorption and emission of two photons. However, they also have some unique characteristics. For the two-photon model, the two photons come from the same mode, while for the two-mode cavity model, the two photons come from different modes. Researchers have studied the two-photon QB. When the initial state of the cavity is a Fock state, at resonance (where the number of photons is twice the number of TLSs), all the radiation energy is transferred to the QB (charging) and back (discharging) [32,33]. It was found that two-photon coupling can increase the average charging power of QBs. However, QBs in the two-mode model have not been studied.

In this paper, a series of two-mode QBs are considered, and the complete description of these QBs is realized. For clarity, we will first consider the case of a single TLS as a battery, avoiding other competing mechanisms based on collective behavior [17,21]. And we will use the rotating-wave-approximation (RWA) method [34] to conduct a simple analysis of a single TLS to study the performance of a QB in the charging and discharging process, including the stored energy and related charging time [32,35–38]. In addition, we will consider the average charging power and fluctuations of stored energy [39]. Next, we will discuss the maximum extractable energy that is stored in the battery and can actually be extracted and used again. This quantity is called ergotropy [40,41] and is usually different from the total energy stored in a battery due to the existence of quantum correlations [22,42]. All these performance parameters will be analyzed under the three different initial conditions for the cavity.

Reference [11] reported that the QBs can be divided into coherent QBs and incoherent QBs according to whether there are nondiagonal elements in the reduced density matrix of batteries, and the competitive relationship between entanglement and ergotropy in incoherent batteries was also discussed qualitatively. In this work, we present the quantitative relationship

*lsy5227@163.com

between the ergotropy and battery-charger entanglement of incoherent QBs and define the resource utilization efficiency $k(t)$ and $k^{\text{ins}}(t)$. Our results suggest that entanglement is a key resource for the high efficiency of such QBs. In addition, we review the differences between some derived models of two-mode QBs. Moreover, in the last section, we extend the above model to multiple TLSs and a cavity with counterrotating terms [8,32].

The organization of this paper is as follows: In Sec. II, we present a two-mode QB in which a single TLS is coupled to a two-mode cavity. In Sec. III, we discuss the performance of two-mode QBs in different initial states. In Sec. IV, we propose some derived models of a two-mode QB (TM), including a two-mode QB dependent on coupling strength (TMD), a two-mode Raman QB (TMR), and a two-mode Raman QB dependent on coupling strength (TMRD), and compare their performances. In Sec. V, we extend the above model and investigate the two-mode Dicke QB (TM-Dicke). In Sec. VI, we draw the conclusions for our work.

II. TWO-MODE QB

We investigate a single QB as a TLS coupled to a two-mode microwave cavity by matter-light interaction. Each transition of the TLS is accompanied by the absorption or emission of a photon from each mode. This simple single battery can be replicated M times, forming a QB that works in a parallel charging configuration [8,34]. The corresponding Hamiltonian can be written as (hereafter we set $\hbar = 1$)

$$\hat{H} = \frac{1}{2}\omega_a\hat{\sigma}_z + \omega_c\hat{a}^\dagger\hat{a} + \omega_c\hat{b}^\dagger\hat{b} + \theta(t)\lambda(\hat{a}^\dagger\hat{b}^\dagger + \hat{a}\hat{b})\hat{\sigma}_x, \quad (1)$$

where a (b) is the annihilation operator of cavity radiation, a^\dagger (b^\dagger) is the creation operator of cavity radiation, $\hat{\sigma}_{x(z)}$ is the Pauli matrix, ω_a is the energy-level spacing of the TLS, and ω_c is the cavity radiation frequency of each mode. $\theta(t)$ is a classical parameter set to 1 during the charging period $[0, \tau]$ and 0 otherwise, representing the external control exerted on the system. Before $t = 0$, there is no interaction between the charger and battery, so the energy exchange cannot be carried out. In the time interval $0 < t < \tau$, the coupled Hamiltonian is turned on, and the two subsystems are coupled together, transferring energy from the cavity to the TLS. The energy stored in the battery is preserved after the interaction is switched off at the moment $t = \tau$. Now we discuss the charging process of a QB in the time interval $0 < t < \tau$.

$|\psi(t)\rangle$ represents the evolution state of the whole system at the moment t . The total energy $E = \langle\psi(t)|\hat{H}|\psi(t)\rangle$ of the QB system is constant at all moments except at the switching points $t = 0$ and $t = \tau$ since the nonzero energy can be transferred to the whole system through external control at these points. (See [34] for a detailed analysis of the energy cost of modulating the interaction.) For simplicity it is assumed that the interacting Hamiltonian is commutative to the local Hamiltonian [43]; therefore, these contributions are equal to zero.

When the intensity of the matter-light interaction λ satisfies $\lambda \ll \omega_a, \omega_c$, the RWA [34] in Eq. (1) can be considered, where the Hamiltonian is expressed as (see Appendix A for the

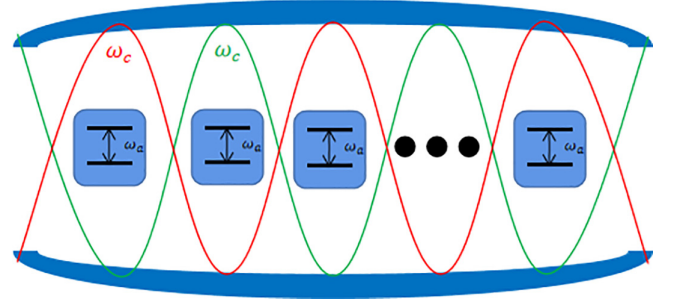


FIG. 1. Scheme of a QB with a set of N identical and independent TLSs with energy separation ω_a between the ground state $|g\rangle$ and the excited state $|e\rangle$, which interacts with a two-mode cavity mode of frequency ω_c via two-photon coupling.

microscopic derivation)

$$\hat{H}^{\text{TM}} = \frac{1}{2}\omega_a\hat{\sigma}_z + \omega_c\hat{a}^\dagger\hat{a} + \omega_c\hat{b}^\dagger\hat{b} + \theta(t)\lambda(\hat{a}^\dagger\hat{b}^\dagger\hat{\sigma}_- + \hat{a}\hat{b}\hat{\sigma}_+), \quad (2)$$

where the first term is the battery represented by the TLS, the middle two terms are the charger represented by the microwave cavity, the last term is the interaction of the TLS with the cavity under the RWA, and

$$\hat{\sigma}_\pm = \frac{\hat{\sigma}_x \pm i\hat{\sigma}_y}{2}, \quad (3)$$

where $\hat{\sigma}_{x(y)}$ is the Pauli matrix.

Next, we focus on the case of resonance $\omega_a = 2\omega_c$ (see Fig. 1). In this case, all the energy associated with the radiation can be transferred to the TLS; otherwise, the energy transfer is zero. This condition ensures the optimal function of the QB, which cannot be achieved in other configurations [32,33].

At time $t = 0$, the initial state of total system is the tensor product state of the TLS and cavity,

$$|\psi(0)\rangle = |g\rangle \otimes \sum_n \alpha_n |n\rangle \otimes \sum_m \alpha_m |m\rangle. \quad (4)$$

The first term represents the TLS in the ground state, the second term represents one of the modes with n photons in the initial state, and the third term represents another mode with m photons in the initial state. We consider the cases in which the initial state of the cavity is in the Fock-Fock state (F-F state), in the Fock-coherent state (F-C state), and in the coherent-coherent state (C-C state). Therefore, we introduce the probability amplitudes α_n ,

$$\alpha_n^{(F)} = \delta_{n,N}, \quad (5)$$

$$\alpha_n^{(C)} = e^{-\frac{N}{2}} \frac{N^{\frac{n}{2}}}{\sqrt{n!}}, \quad (6)$$

where the superscript F and C represent the Fock state and coherent state, respectively. For the Fock state, N represents the number of photons precisely, while for the coherent state, N represents the average number of photons.

III. PERFORMANCE OF A TWO-MODE QB

We now investigate the performance of a two-mode QB and compare the three different cavity initial states mentioned in the previous section.

In order to study the performance of a QB, it is necessary to study the evolution state of the whole system at any time under the initial state in Eq. (4). We observe that in the base vector given by $|g\rangle \otimes |n\rangle \otimes |m\rangle$ and $|e\rangle \otimes |n-1\rangle \otimes |m-1\rangle$ ($n > 1, m > 1$), the Hamiltonian in Eq. (2) can be simply rewritten as

$$\hat{H}^{(n,m)} = \begin{pmatrix} \frac{\omega_a}{2}(n+m-1) & \lambda\sqrt{nm} \\ \lambda\sqrt{nm} & \frac{\omega_a}{2}(n+m-1) \end{pmatrix}, \quad (7)$$

where n and m represent the actual photon numbers in each mode of the two-mode cavity. The dynamic evolution of the whole system is still limited to a two-dimensional space. The eigenstates of Hamiltonian (7) are

$$|\psi_{\pm}^{(n,m)}\rangle = \frac{|g\rangle \otimes |n\rangle \otimes |m\rangle \pm |e\rangle \otimes |n-1\rangle \otimes |m-1\rangle}{\sqrt{2}}. \quad (8)$$

The eigenvalues are

$$E_{\pm}^{(n,m)} = \frac{\omega_a}{2}(n+m-1) \pm \lambda\sqrt{nm}. \quad (9)$$

From these equations, we can transform Eq. (4) into

$$|\psi(0)\rangle = \sum_{n,m} \alpha_n \alpha_m \left(\frac{|\psi_+^{(n,m)}\rangle + |\psi_-^{(n,m)}\rangle}{\sqrt{2}} \right). \quad (10)$$

Therefore, the state function at any time can be expressed as $|\psi(t)\rangle = e^{-i\hat{H}t} |\psi(0)\rangle$.

In our study, the evolution behavior of the reduced density matrix over time is very important. Therefore, we can obtain $\rho_{\text{TLS}}(t) = \text{Tr}_C(|\psi(t)\rangle \langle \psi(t)|)$, which is the reduced density matrix of the TLS at any time, where C represents the partial trace of the cavity in the whole-system density matrix $\rho(t) = |\psi(t)\rangle \langle \psi(t)|$.

A. Stored energy and average power

The energy stored in the QB at time t is [8,32,36,44]

$$\Delta E(t) = E(t) - E(0), \quad (11)$$

where $E(t) = \langle \psi(t) | \hat{H}_{\text{QB}} | \psi(t) \rangle$ is the energy of the QB at time t and \hat{H}_{QB} is the battery-related part of the total Hamiltonian in Eq. (2),

$$\hat{H}_{\text{QB}} = \frac{\omega_a}{2} \hat{\sigma}_z. \quad (12)$$

Inserting the time-evolved state of the battery into Eq. (11) we have

$$\Delta E(t) = \omega_a \sum_{n,m} P_n P_m \sin^2(\lambda\sqrt{nm}t), \quad (13)$$

where $P_{n(m)} = \sum_{n(m)} |\alpha_{n(m)}|^2$.

An important task for QBs is to store the most energy in the fastest time. From this perspective, the maximum energy stored can be defined as [32,34]

$$\Delta E_{\text{max}} = \max_t [\Delta E(t)] = \Delta E(t_E), \quad (14)$$

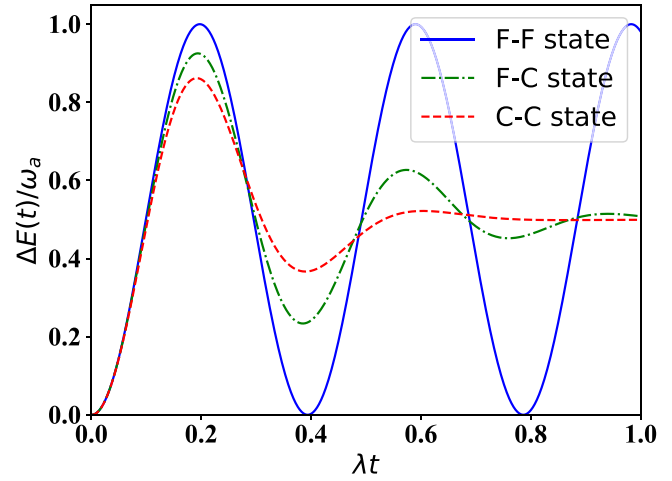


FIG. 2. Behavior of stored energy $\Delta E(t)$ over time. The initial state of the two-mode cavity is in the F-F state (blue solid line), in the F-C state (green dot-dashed line), or in the C-C state (red dashed line); the average photon number is $N = M = 8$.

where t_E is the time when the maximum stored energy occurs. When the cavity is in the F-F state ($\alpha_{n(m)}^F = \delta_{n(m),N(M)}$) at the initial moment and $\sin^2(\lambda\sqrt{nm}t) = 1$, one can analytically calculate the time it takes for t_E ,

$$t_E^{\text{F-F}} = \frac{(k + \frac{1}{2})\pi}{\lambda\sqrt{nm}}, \quad (15)$$

$k \in \mathbb{R}$. On the contrary, the corresponding time t_E can be obtained using a numerical method for the case in which the cavity is in the F-C state and the C-C state at the initial moment.

In Fig. 2, we show the evolution of stored energy $\Delta E(t)$ over time for three different initial states [see Eq. (13)]; the unit is ω_a , and the average photon number is $N = M = 8$. From Fig. 2, we can see that the battery can reach a fully charged state ($\Delta E_{\text{max}}^{\text{F-F}} = \omega_a$) only when the two-mode cavity is in the F-F state. However, when the cavity is in the F-C state with the same average number of photons ($N = M = 8$), the maximum storage energy can reach $0.93\omega_a$. When the initial state of the two-mode cavity is in the C-C state, the charging energy can reach only $0.86\omega_a$. This has guiding significance for the experimental realization of such QBs [45].

In addition, the minimum charging times are comparable in the cases of the two-mode cavity in the F-F state and C-C state ($N = M = 8$). In fact, from Eq. (15), we get $\lambda t_E^{\text{F-F}} \sim 0.196$, $\lambda t_E^{\text{F-C}} \sim 0.193$, and $\lambda t_E^{\text{C-C}} \sim 0.192$. From the previous discussion, it can be concluded that the F-F state is the best choice for the initial state of the charger to store all energy in the battery in the shortest time [33,34]. It is worth noting that for a given quantum state of the charger, the charging time in the two-mode QB is usually shorter than the corresponding charging time in the two-photon case with the same average photon number [32,33]. In fact, as mentioned in the Ref. [33], the energy of the two-photon process is given by $\Delta E(t) = \omega_a \sum_n P_n \sin^2[\lambda\sqrt{n(n-1)}t]$, which means that the ratio of time required for the maximum energy to be charged is $1/\sqrt{n(n-1)}$. For the two-mode QB, the ratio of time is $1/\sqrt{nm}$. Therefore, the charging time of the two-mode QB is

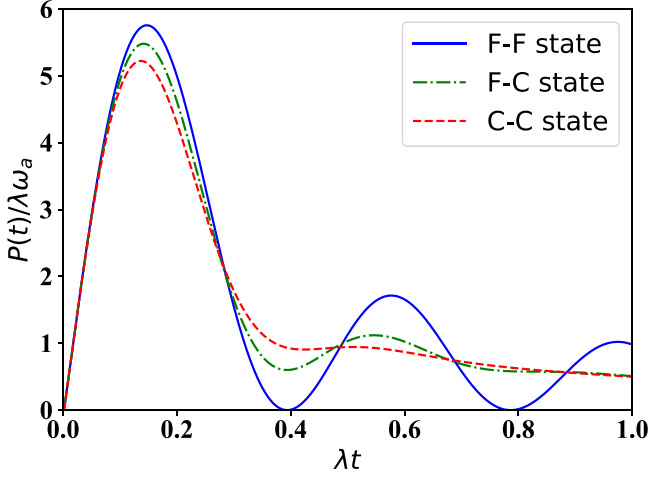


FIG. 3. Behavior of average power $P(t)$ over time. The initial state of the two-mode cavity is in the F-F state (blue solid line), in the F-C state (green dot-dashed line), or in the C-C state (red dashed line); the average photon number is $N = M = 8$.

faster than that of the two-photon QB with other parameters being constant.

Another related performance parameter is average charging power, which is defined as [8,26,44]

$$P(t) = \frac{\Delta E(t)}{t}. \quad (16)$$

In this case, we are interested in achieving the maximum charging power in the shortest possible time. Therefore, we need to consider the maximum charging power [8,32,34]

$$P_{\max} = \max_t [P(t)] = P(t_P), \quad (17)$$

where t_P represents the time when the charging power reaches the maximum value.

In Fig. 3, we show the evolution of average power $P(t)$ over time for three different initial states [see Eq.(16)]; the unit is $\lambda\omega_a$, and the average photon number is $N = M = 8$. Furthermore, we find that this quantity reaches the largest value when the two-mode cavity is in the F-F state ($P_{\max}^{\text{F-F}} = 5.76\lambda\omega_a$) and decreases in the F-C state ($P_{\max}^{\text{F-C}} = 5.48\lambda\omega_a$) with the same average photon number and in the C-C state ($P_{\max}^{\text{C-C}} = 5.22\lambda\omega_a$). However, the times to reach their maxima are very close ($\lambda t_E^{\text{F-F}} \sim 0.146$, $\lambda t_E^{\text{F-C}} \sim 0.140$, and $\lambda t_E^{\text{C-C}} \sim 0.138$).

B. Energy fluctuations

In order to get a complete description of the performance of the two-mode QB, we also need to evaluate the quantum fluctuations associated with stored energy since it can affect the charging performance negatively. We can discuss the stability of the charging process according to the fluctuation of stored energy in the same time interval, which can be expressed as [32,36,45]

$$\begin{aligned} \Xi^2(t) &= \langle \psi(0) | [\hat{H}_{\text{QB}}(t) - \hat{H}_{\text{QB}}(0)]^2 | \psi(0) \rangle \\ &\quad - \{ \langle \psi(0) | [\hat{H}_{\text{QB}}(t) - \hat{H}_{\text{QB}}(0)] | \psi(0) \rangle \}^2 \\ &= \Delta E(t)[\omega_a - \Delta E(t)], \end{aligned} \quad (18)$$

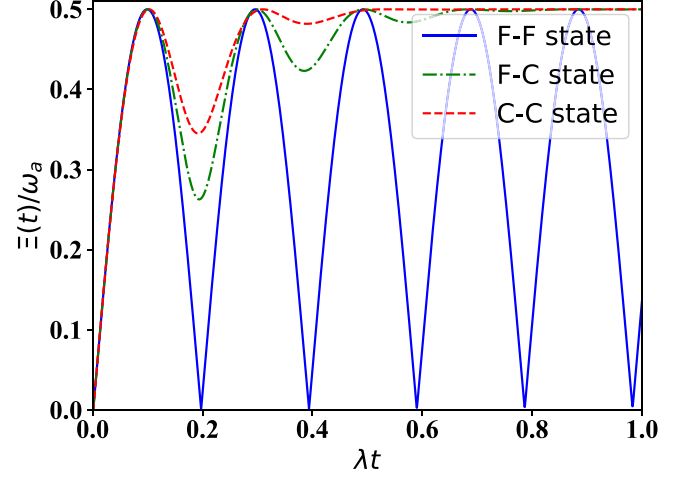


FIG. 4. Behavior of energy fluctuations $\Xi(t)$ over time. The initial state of the two-mode cavity is in the F-F state (blue solid line), in the F-C state (green dot-dashed line), or in the C-C state (red dashed line); the average photon number is $N = M = 8$.

where $|\psi(0)\rangle$ is the initial state in Eq. (10) and \hat{H}_{QB} is the evolution of the TLS Hamiltonian over time in the Heisenberg picture.

In Fig. 4, we show the evolution of $\Xi(t)$ over time for three different initial states. We are interested in the value $\Xi(t)$ at the moment t_E when the stored energy reaches its maximum and try to understand how it affects the performance of the QB. At t_E , the energy fluctuation is defined as [33]

$$\Xi(t_E) = \bar{\Xi}. \quad (19)$$

It can be seen that when the charging energy reaches the maximum value, the energy fluctuation is zero ($\bar{\Xi}^{\text{F-F}} = 0$) for the case in which the two-mode cavity is in the F-F state. This can be understood from Eq. (18). When the stored energy reaches its maximum value, the whole system (battery and charger) is in a separable state $|\psi(t_E)\rangle = |e\rangle \otimes |n-1\rangle \otimes |m-1\rangle$. However, this is not true for the cases in which the two-mode cavity is in the F-C state and the C-C state. When the stored energy reaches its maximum, the energy fluctuation is nonzero. Because in these two initial states the two-mode QB cannot be fully charged, they do not reach $\bar{\Xi} = 0$. In fact, for the two-mode cavity in the F-C state, we get $\bar{\Xi}^{\text{F-C}} = 0.26\omega_a$, and for the C-C state, we have $\bar{\Xi}^{\text{C-C}} = 0.35\omega_a$.

It is confirmed again that the Fock state is the best initial state for building a QB with good performance. In fact, this particular initial state is unaffected by fluctuations in stored energy.

C. Ergotropy

Another performance parameter related to QB efficiency that needs to be studied is ergotropy [5,41]. It contains the maximum amount of stored energy that can be converted into usable work and can be extracted from the QB as it evolves. In general, this ergotropy is not the same as stored energy. Because some of the stored energy may be locked up in correlation, it cannot be extracted [41]. The general derivation of this quantity starts with the Hamiltonian for the QB, written

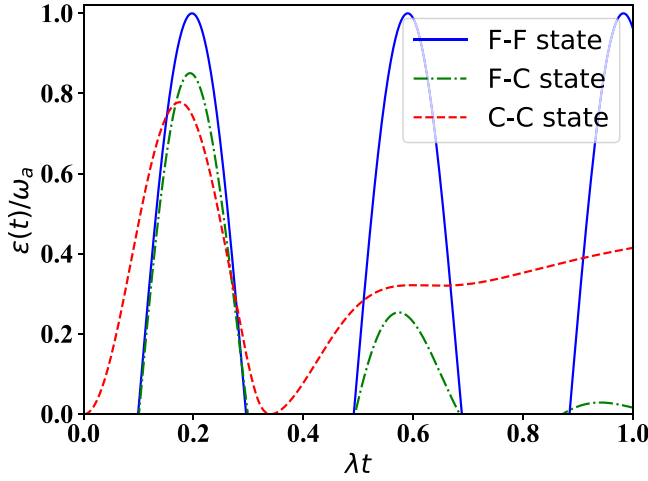


FIG. 5. Behavior of ergotropy $\varepsilon(t)$ over time. The initial state of the two-mode cavity is in the F-F state (blue solid line), in the F-C state (green dot-dashed line), or in the C-C state (red dashed line); the average photon number is $N = M = 8$.

as [5]

$$\hat{H}_{\text{QB}} = \sum_n \epsilon_n |\epsilon_n\rangle \langle \epsilon_n|, \quad (20)$$

where the energy eigenvalues are arranged in order $\epsilon_n < \epsilon_{n+1}$, $|\epsilon_n\rangle$ are the eigenvectors, and the density matrix at a given time is

$$\rho_{\text{TLS}}(t) = \sum_n r_n(t) |r_n(t)\rangle \langle r_n(t)|, \quad (21)$$

where $r_n > r_{n+1}$ and $|r_n(t)\rangle$ are the eigenvectors. The maximum work that can be extracted from the QB after a period of time t is called ergotropy, which can be written as [40]

$$\varepsilon(t) = \sum_{j,k} r_j(t) \epsilon_k [| \langle r_j(t) | \epsilon_k \rangle |^2 - \delta_{j,k}]. \quad (22)$$

When $j = k$, $\delta_{j,k} = 1$; otherwise, $\delta_{j,k} = 0$.

When the initial state of the system is a passive state, we cannot extract work from it, $\varepsilon = 0$. In general, the ergotropy reaches its maximum ε_{th} when the final state of the system is the thermal state $\rho_{\text{TLS}} = e^{-\beta H_{\text{QB}}} / Z$ (β is the inverse temperature of the system and $Z = \text{Tr} e^{-\beta H_{\text{QB}}}$). Therefore, the range of ergotropy is $0 < \varepsilon < \varepsilon_{\text{th}}$ [40].

Now we try to find an expression for the ergotropy of our system. To do this, we need to diagonalize the density matrix of the TLS in the equation for $\rho_{\text{TLS}}(t)$. Its eigenvalues are

$$r_s(t) = \frac{1 + (-1)^s \sqrt{1 - 4 \det \rho_{\text{TLS}}(t)}}{2}, \quad (23)$$

where $s = 0, 1$. In addition, the eigenvalue of \hat{H}_{QB} in Eq. (12) is $\epsilon_s = (-1)^s \omega_a / 2$. Therefore, substituting $r_s(t)$ and $\epsilon_s(t)$ into Eq. (22), the ergotropy at time t can be obtained,

$$\varepsilon(t) = E(t) - \sum_{s=0,1} r_s(t) \epsilon_s = E(t) - \frac{\omega_a}{2} \sqrt{1 - 4 \det \rho_{\text{TLS}}(t)}. \quad (24)$$

Figure 5 illustrates the evolution of ergotropy $\varepsilon(t)$ over time. We can see that the behavior of ergotropy over time is similar

to that of the stored energy. We can also observe that the ergotropy can reach the maximum only when the initial state of the two-mode cavity is in the F-F state ($\varepsilon_{\text{max}} = \omega_a$). This occurs at the moment $t_E^{\text{F-F}}$ when the stored energy reaches its maximum and the TLS is in a pure state, which also indicates the relevant properties of the cavity state.

Based on previous research [11], we know that the battery can be divided into coherent QBs and incoherent QBs, according to whether there is a nondiagonal element in the reduced density matrix of the TLS. Because of the vanishing coherence, the final extractable work is dependent on the battery-charger entanglement and is negatively correlated in incoherent QBs. Incoherent QBs are promising candidates; due to the vanishing entanglement and coherence of the charged battery, it can achieve the optimal ergotropy. For the three different initial states of the two-mode QB, the battery is an incoherent QB only when the cavity is in the F-F state due to the disappearance of nondiagonal elements in the reduced density matrix of the TLS (see Appendix B for more details). Next, we will further investigate the effects of entanglement in the above situation. For a bipartite pure state, the battery-charger entanglement is characterized by von Neumann entropy of the reduced density matrix of batteries,

$$S(t) = -\text{Tr}\{\rho_{\text{TLS}}(t) \log_2[\rho_{\text{TLS}}(t)]\}, \quad (25)$$

where $\rho_{\text{TLS}}(t)$ is the reduced density matrix of the TLS and

$$\rho_{\text{TLS}}(t) = \begin{pmatrix} \cos^2(\lambda\sqrt{nm}t) & 0 \\ 0 & \sin^2(\lambda\sqrt{nm}t) \end{pmatrix}, \quad (26)$$

where $\cos^2(\lambda\sqrt{nm}t)$ and $\sin^2(\lambda\sqrt{nm}t)$ represent the populations in the low-energy state and high-energy state, respectively. So we define $r(t) = \cos^2(\lambda\sqrt{nm}t) - \sin^2(\lambda\sqrt{nm}t)$ to represent the difference between populations in the low-energy state and high-energy state, that is, the occupation numbers for the battery part.

Inserting $r(t)$ into Eqs. (22) and (25), respectively, we have

$$\varepsilon(t) = \begin{cases} 0 & r(t) \geq 0, \\ -\omega_a r(t) & r(t) < 0, \end{cases} \quad (27)$$

$$S(t) = -\frac{1+r(t)}{2} \log_2 \frac{1+r(t)}{2} - \frac{1-r(t)}{2} \log_2 \frac{1-r(t)}{2}. \quad (28)$$

Figure 6 shows the occupation numbers for battery part $r(t)$, stored energy $\Delta E(t)$, ergotropy $\varepsilon(t)$, and entanglement $S(t)$ evolution over time when the cavity is in the F-F state. We find that the entanglement of the battery and charger is increased during the energy-storage stage. And at this stage, the excitation of the TLS from the low-energy states to high-energy states continues, until the population of the battery part displays a nearly balanced distribution. Further excitation will induce the population inversion and lead to a decrease in entanglement. Therefore, at the end of the charging process, the vanishing entanglement indicates that the battery is located in a high-energy state and thus leads to optimal ergotropy. In addition, we believe that entanglement is a key resource in the energy-extraction stage. That is to say, the more entanglement is consumed, the more energy can be extracted. In order to measure the quantitative relationship between entanglement and ergotropy in the above stage, we introduce the average

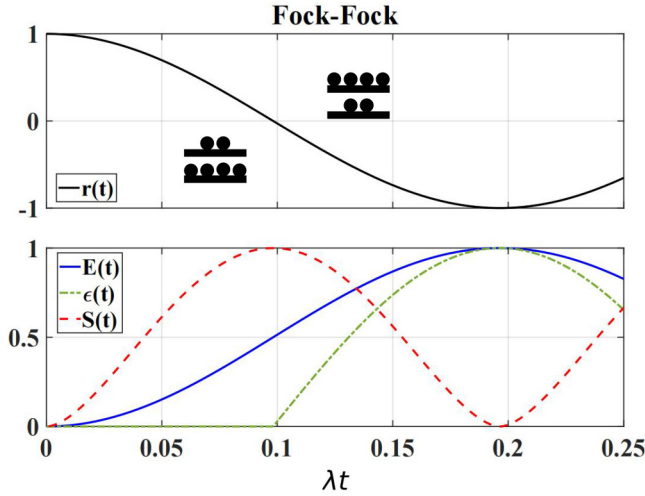


FIG. 6. Behavior of the occupation numbers for the battery part $r(t)$ (black solid line), stored energy $\Delta E(t)$ (blue solid line), ergotropy $\varepsilon(t)$ (green dot-dashed line), and entanglement $S(t)$ (red dashed line) over time when the initial state of the two-mode cavity is in the F-F state; the average photon number is $N = M = 8$. The illustration consisting of black horizontal lines and black balls is a schematic diagram of the proportions of the TLS. The black horizontal lines represent the two levels of the TLS, with the lower horizontal line being the low-energy state and the upper horizontal line being the high-energy state. The black balls indicate the proportions of the TLS in the high-energy state and low-energy state. The more balls there are, the larger the proportion is and vice versa. If the numbers of balls are equal, the proportions of high-energy and low-energy states are equal.

resource utilization efficiency,

$$k(t) = \left| \frac{\Delta \varepsilon(t)}{\Delta S(t)} \right| = -\frac{\omega_a r(t)}{\frac{1+r(t)}{2} \log_2 \frac{1+r(t)}{2} + \frac{1-r(t)}{2} \log_2 \frac{1-r(t)}{2} + 1}. \quad (29)$$

Figure 7 shows the $k(t)$ and $k^{\text{ins}}(t)$ evolution over time. In the initial stage of ergotropy increasing, $\Delta S(t)$ tends to zero, and $k(t)$ tends to infinity. We can also observe that k rapidly approaches 1 over time. This confirms that there is a nearly linear relationship between ergotropy and entanglement; namely, consuming unit entanglement generates unit ergotropy.

To further investigate the utilization efficiency of entanglement at each moment, we introduce the instantaneous resource utilization efficiency,

$$k^{\text{ins}}(t) = \left| \frac{d\varepsilon(t)}{dS(t)} \right|. \quad (30)$$

From Fig. 7, we can also observe that throughout the entire stage of energy extraction, $k^{\text{ins}}(t)$ and $k(t)$ have the same trend, and they both tend to infinity in the initial stage. Moreover, $k^{\text{ins}}(t)$ is less than $k(t)$ at any time. From Fig. 7, we can also see that in the initial stage of ergotropy increasing, $k^{\text{ins}}(t)$ is relatively large. It quickly approaches zero over time. This indicates that in the initial stage, the utilization efficiency of

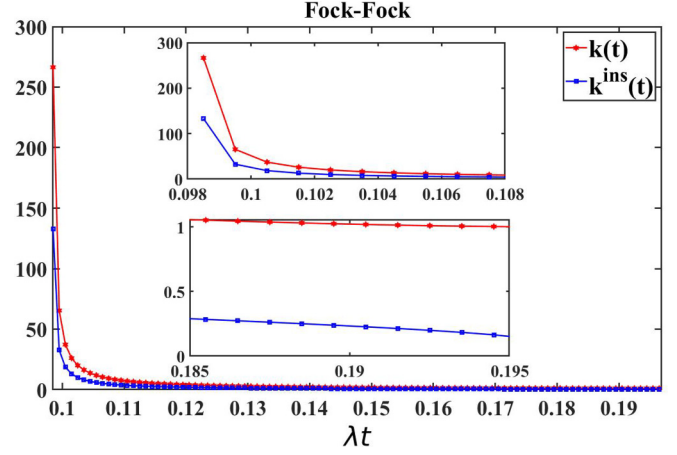


FIG. 7. Behavior of $k(t)$ and $k^{\text{ins}}(t)$ over time when the initial state of the two-mode cavity is in the F-F state; the average photon number is $N = M = 8$.

entanglement is very high. Consuming unit entanglement can extract a large amount of energy. However, resource utilization efficiency rapidly decreases over time. $k^{\text{ins}}(t)$ and $k(t)$ provide us with a complete description of resource utilization efficiency.

To better quantify the actual proportion of extractable energy, we now evaluate the ratio between ergotropy and stored energy,

$$\eta(t) = \frac{\varepsilon(t)}{\Delta E(t)} = 1 - \frac{\omega_a}{2\Delta E(t)} [1 - \sqrt{1 - 4 \det \rho_{\text{TLS}}(t)}]. \quad (31)$$

In Fig. 8, we compare the evolution of $\eta(t)$ over time for three different initial states. It can be observed that the stored energy can be almost completely extracted and used as usable energy in a relatively short time for the two-mode cavity in the C-C state. However, the amount of energy stored in the system is very small during this time (see Fig. 2). For the two-mode

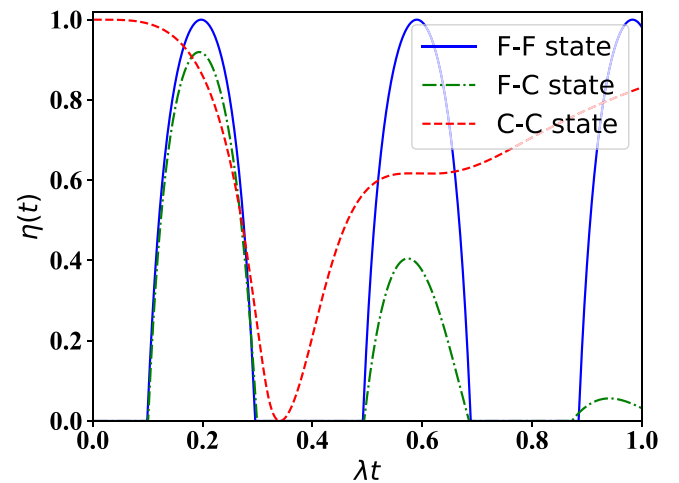


FIG. 8. Behavior of $\eta(t)$ over time. The initial state of the two-mode cavity is in the F-F state (blue solid line), in the F-C state (green dot-dashed line), or in the C-C state (red dashed line); the average photon number is $N = M = 8$.

TABLE I. Expressions for the stored energy $\Delta E(t)$, average power $P(t)$, and ergotropy $\varepsilon(t)$ over time for the two-mode QB, the two-mode QB dependent on coupling strength, the two-mode Raman QB, and the two-mode Raman QB dependent on coupling strength.

| Model | Parameter | | |
|--|--|--|---|
| | Stored energy $\Delta E(t)$ | Average power $P(t)$ | Ergotropy $\varepsilon(t)$ |
| Two-mode QB | $\omega_a \sin^2(\lambda\sqrt{nm}t)$ | $\frac{\omega_a \sin^2(\lambda\sqrt{nm}t)}{t}$ | $-2\omega_a \cos(2\lambda\sqrt{nm}t)$ |
| Two-mode QB dependent on coupling strength | $\omega_a \sin^2[\lambda\sqrt{nmn(m-1)}t]$ | $\frac{\omega_a \sin^2[\lambda\sqrt{nmn(m-1)}t]}{t}$ | $-2\omega_a \cos[2\lambda\sqrt{nmn(m-1)}t]$ |
| Two-mode Raman QB | $\omega_a \sin^2[\lambda\sqrt{n(m+1)}t]$ | $\frac{\omega_a \sin^2[\lambda\sqrt{n(m+1)}t]}{t}$ | $-2\omega_a \cos[2\lambda\sqrt{n(m+1)}t]$ |
| Two-mode Raman QB dependent on coupling strength | $\omega_a \sin^2[\lambda\sqrt{n(m+1)n(m+1)}t]$ | $\frac{\omega_a \sin^2[\lambda\sqrt{n(m+1)n(m+1)}t]}{t}$ | $-2\omega_a \cos[2\lambda\sqrt{n(m+1)n(m+1)}t]$ |

cavity in the F-F state, the stored energy can be fully extracted only within a corresponding short period of time $t_E^{\text{F-F}}$. The advantage is that the stored energy is close or equal to the maximum value ($\Delta E_{\text{max}}^{\text{F-F}} = \omega_a$).

IV. THE TWO-MODE RAMAN QB

When the coupling intensity between the TLS and cavity depends on the intensity of the cavity, we choose a special model which was first introduced in Ref. [46]. In particular, this type of model is interesting because of its inherent connection to an SU(1,1) Jaynes-Cummings (JC) model and can be written as a combination of generators of SU(1,1) algebra [47]. The Hamiltonian of the two-mode QB dependent on coupling strength (TMD) can be expressed as ($\omega_a = 2\omega_c$; see Appendix A for the reason why we choose the special form) [31]

$$\hat{H}^{\text{TMD}} = \frac{1}{2}\omega_a\hat{\sigma}_z + \omega_c\hat{a}^\dagger\hat{a} + \omega_c\hat{b}^\dagger\hat{b} + \theta(t)\lambda(\hat{L}_- + \hat{L}_+),$$

$$\hat{L}_- = \sqrt{\hat{a}^\dagger\hat{a}}\hat{a}^\dagger\hat{b}^\dagger\sqrt{\hat{b}^\dagger\hat{b}}\hat{\sigma}_-, \quad \hat{L}_+ = \sqrt{\hat{b}^\dagger\hat{b}}\hat{b}^\dagger\hat{a}^\dagger\sqrt{\hat{a}^\dagger\hat{a}}\hat{\sigma}_+. \quad (32)$$

The base vector is $|g\rangle \otimes |n\rangle \otimes |m\rangle$ and $|e\rangle \otimes |n-1\rangle \otimes |m-1\rangle$ ($n > 1, m > 1$).

Raman scattering is an important nonlinear process of the interaction between the atoms and cavity. Since the study of Raman scattering can reveal many nonclassical characteristics of the interaction between the atoms and cavity, we also consider the two-mode Raman model under the conditions of the QB and describe the performance of this kind of model. The atom in the high- Q cavity has two nondegenerate energy levels, $|e\rangle$ and $|g\rangle$, which interacts with the two-mode cavity through the virtual energy level $|j\rangle$, and in the RWA, the Hamiltonian of the two-mode Raman QB (TMR) in the above process is expressed as ($\omega_a = \omega_b - \omega_c$) [29]

$$\hat{H}^{\text{TMR}} = \frac{1}{2}\omega_a\hat{\sigma}_z + \omega_b\hat{a}^\dagger\hat{a} + \omega_c\hat{b}^\dagger\hat{b} + \theta(t)\lambda(\hat{a}^\dagger\hat{b}\hat{\sigma}_- + \hat{b}^\dagger\hat{a}\hat{\sigma}_+). \quad (33)$$

The base vector is $|g\rangle \otimes |n\rangle \otimes |m\rangle$ and $|e\rangle \otimes |n-1\rangle \otimes |m+1\rangle$ ($n > 1, m > 1$).

The Hamiltonian of the two-mode Raman QB dependent on coupling strength (TMRD) is ($\omega_a = \omega_b - \omega_c$) [29,31]

$$\hat{H}^{\text{TMRD}} = \frac{1}{2}\omega_a\hat{\sigma}_z + \omega_b\hat{a}^\dagger\hat{a} + \omega_c\hat{b}^\dagger\hat{b} + \theta(t)\lambda(\hat{L}_- + \hat{L}_+),$$

$$\hat{L}_- = \sqrt{\hat{a}^\dagger\hat{a}}\hat{a}^\dagger\hat{b}^\dagger\sqrt{\hat{b}^\dagger\hat{b}}\hat{\sigma}_-, \quad \hat{L}_+ = \sqrt{\hat{b}^\dagger\hat{b}}\hat{b}^\dagger\hat{a}^\dagger\sqrt{\hat{a}^\dagger\hat{a}}\hat{\sigma}_+. \quad (34)$$

The base vector is $|g\rangle \otimes |n\rangle \otimes |m\rangle$ and $|e\rangle \otimes |n-1\rangle \otimes |m+1\rangle$ ($n > 1, m > 1$).

The performance of QBs in the above three models is shown in Table I. From Table I, we can see that the ratio of time required for the two-mode QB to reach the maximum energy is $1/\sqrt{nm}$, and for the two-mode Raman QB, the ratio is $1/\sqrt{(n+1)m}$. Under the same conditions, the charging time of the two-mode Raman QB is faster. Table I also shows that the model related to coupling strength has shorter charging time and higher charging efficiency than the original model. Among these derived models, the two-mode Raman QB dependent on coupling strength has the best performance.

In Fig. 9, we show the behavior of stored energy, average power, and ergotropy for the above four models. Figure 9 shows that all four models can reach a fully charged state. At the moment t_E the energy fluctuation is zero. Since the Raman scattering and coupling strength can both improve the performance of batteries, the two-mode Raman QB dependent on coupling strength exhibits the optimal performance.

To quantify the utilization efficiency of entanglement in the energy-extraction stage of QBs in the four different models mentioned above, we calculate $k(t)$ and $k^{\text{ins}}(t)$ separately. From Eqs. (29) and (30), we can see that $k(t)$ and $k^{\text{ins}}(t)$ are functions of $r(t)$. The $r(t)$ functions corresponding to QBs in the four different models mentioned above are

$$r^{\text{TM}}(t) = \cos^2(\lambda\sqrt{nm}t) - \sin^2(\lambda\sqrt{nm}t),$$

$$r^{\text{TMD}}(t) = \cos^2[\lambda\sqrt{nmn(m-1)}t] - \sin^2[\lambda\sqrt{nmn(m-1)}t],$$

$$r^{\text{TMR}}(t) = \cos^2[\lambda\sqrt{n(m+1)}t] - \sin^2[\lambda\sqrt{n(m+1)}t],$$

$$r^{\text{TMRD}}(t) = \cos^2[\lambda\sqrt{n(m+1)n(m+1)}t] - \sin^2[\lambda\sqrt{n(m+1)n(m+1)}t]. \quad (35)$$

Figure 10 shows the evolution of $k(t)$ and $k^{\text{ins}}(t)$ over time for the above four models. We can see that the properties of $k(t)$ and $k^{\text{ins}}(t)$ in the other three QBs in the different models are consistent with those of the two-mode QB. We can also see that the resource utilization efficiency of the two-mode Raman QB dependent on coupling strength is the highest, which means that the most energy can be extracted using entanglement in the shortest time. This can also be explained by Eq. (35) because, with all parameters determined, the ratio of time required for the maximum energy is the shortest. Again, this confirms that the performance of the two-mode Raman QB dependent on coupling strength is the best.

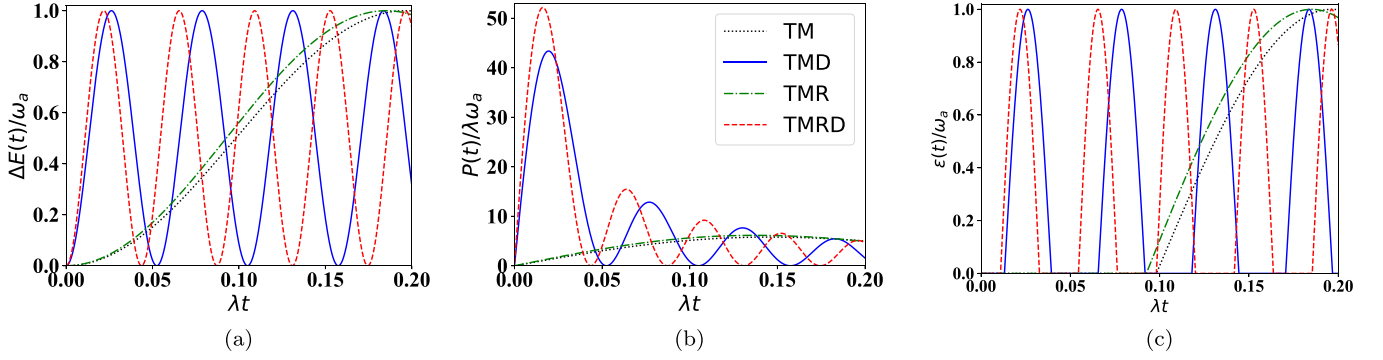


FIG. 9. Behavior of the stored energy $\Delta E(t)$, average power $P(t)$, and ergotropy $\varepsilon(t)$ with time for the two-mode QB (black dotted line), the two-mode QB dependent on coupling strength (blue solid line), the two-mode Raman QB (green dot-dashed line), and the two-mode Raman QB dependent on coupling strength (red dashed line); the average photon number is $N = M = 8$.

V. TWO-MODE DICKE QB

We consider a QB modeled as a finite set of N , with identical and independent TLSs coupled to a two-mode cavity. The counterrotating terms are also considered. The system can be described using the so-called Dicke model [48]. In particular, we want to consider N TLSs coupled to a two-mode cavity via a two-photon coupling (TM-Dicke), for which the Hamiltonian is [49,50]

$$\hat{H}^{\text{TM-Dicke}} = \omega_a \hat{J}_z + \omega_c \hat{a}^\dagger \hat{a} + \omega_c \hat{b}^\dagger \hat{b} + \theta(t) \lambda (\hat{a}^\dagger \hat{b}^\dagger + \hat{a} \hat{b}) \hat{J}_x. \quad (36)$$

The notation

$$\hat{J}_\alpha = \frac{1}{2} \sum_{i=1}^N \hat{\sigma}_i^\alpha, \quad (37)$$

with $\alpha = x, y, z$, represents the components of a pseudospin operator expressed in terms of the Pauli matrix of the i th TLS.

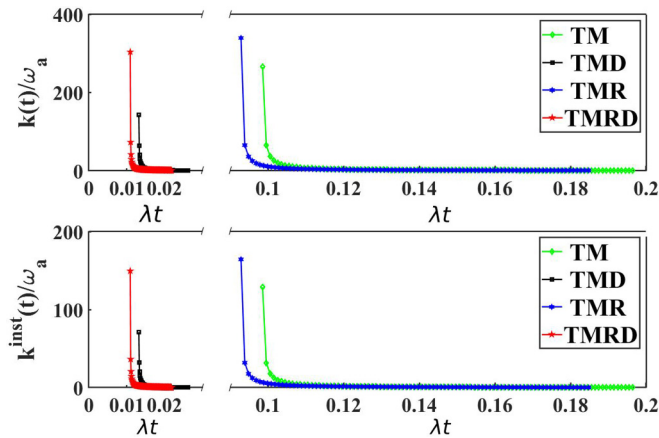


FIG. 10. Behavior of $k(t)$ and $k^{\text{inst}}(t)$ with time for the two-mode QB (green line with diamonds), the two-mode QB dependent on coupling strength (black line with squares), the two-mode Raman QB (blue line with stars), and the two-mode Raman QB dependent on coupling strength (red line with stars); the average photon number is $N = M = 8$.

Next, we consider initial states of the form

$$|\psi(0)\rangle = \underbrace{|g, \dots, g\rangle}_N \otimes |2N\rangle \otimes |2N\rangle. \quad (38)$$

The N TLSs are prepared in the ground state $|g\rangle$, and the cavity modes are both in the $2N$ Fock states.

Next, we will analyze what happens to the performance of a two-mode Dicke QB in the weak-coupling regime and the ultrastrong-coupling (USC) regime [51,52]. We will also compare our results with those obtained with the Tavis-Cummings (TC) model (TM-TC) and the two-photon Dicke model (TP-Dicke). The corresponding Hamiltonians are ($\omega_a = 2\omega_c$)

$$\begin{aligned} \hat{H}^{\text{TM-TC}} &= \omega_a \hat{J}_z + \omega_c \hat{a}^\dagger \hat{a} + \omega_c \hat{b}^\dagger \hat{b} + \theta(t) \lambda (\hat{a}^\dagger \hat{b}^\dagger \hat{\sigma}_- + \hat{a} \hat{b} \hat{\sigma}_+), \\ \hat{H}^{\text{TP-Dicke}} &= \omega_a \hat{J}_z + \omega_c \hat{a}^\dagger \hat{a} + \theta(t) \lambda \hat{J}_x [(\hat{a}^\dagger)^2 + (\hat{a})^2]. \end{aligned} \quad (39)$$

In the first case, considering weak coupling $\lambda \ll \omega_a$, we consider $\lambda = 0.005\omega_a$ as a representative value; other coupling constants in this regime lead to similar results. In Fig. 11(a) we report the stored energy $\Delta E(t)$ for a given number of TLSs, $N = 10$, for two-mode Dicke, two-mode TC, and two-photon Dicke coupling, respectively. From Fig. 11(a), we can see that the maximum stored energy in the two-mode Dicke case ($\Delta E_{\text{max}}^{\text{(TM-Dicke)}}/N\omega_a \sim 0.950$) is higher than the two-photon one ($\Delta E_{\text{max}}^{\text{(TP-Dicke)}}/N\omega_a \sim 0.710$). In addition, the charging time in the two-mode Dicke case is $\omega_a t_E^{\text{(TM-Dicke)}} = 20.4$, and in the two-photon Dicke case it is way faster ($\omega_a t_E^{\text{(TP-Dicke)}} = 19.4$). From Fig. 11(d), we can see an enhancement of the maximum of the averaged charging power in the two-mode Dicke case $P_{\text{max}}^{\text{(TM-Dicke)}}/N^2\omega_a^2 \sim 0.006$ compared to the one in the two-photon Dicke case, where $P_{\text{max}}^{\text{(TP-Dicke)}}/N^2\omega_a^2 \sim 0.005$, which proves the better performance of the two-mode Dicke model. In Figs. 11(a) and 11(d), we can also see smooth oscillations for the two-mode Dicke model (red solid line), which are in full agreement with the result obtained for the two-mode TC model (black dotted line). This analysis allows us to understand that the counterrotating terms do not provide an advantage for the performance of the two-mode QB in the weak-coupling regime.

We now discuss coupling strengths in the USC regime, namely, with higher values of λ up to $\lambda \lesssim \omega_a$ [51,52], and compare the results with those for the weak-coupling case. In Figs. 11(b) and 11(e), we report the behavior of $\Delta E(t)$ and

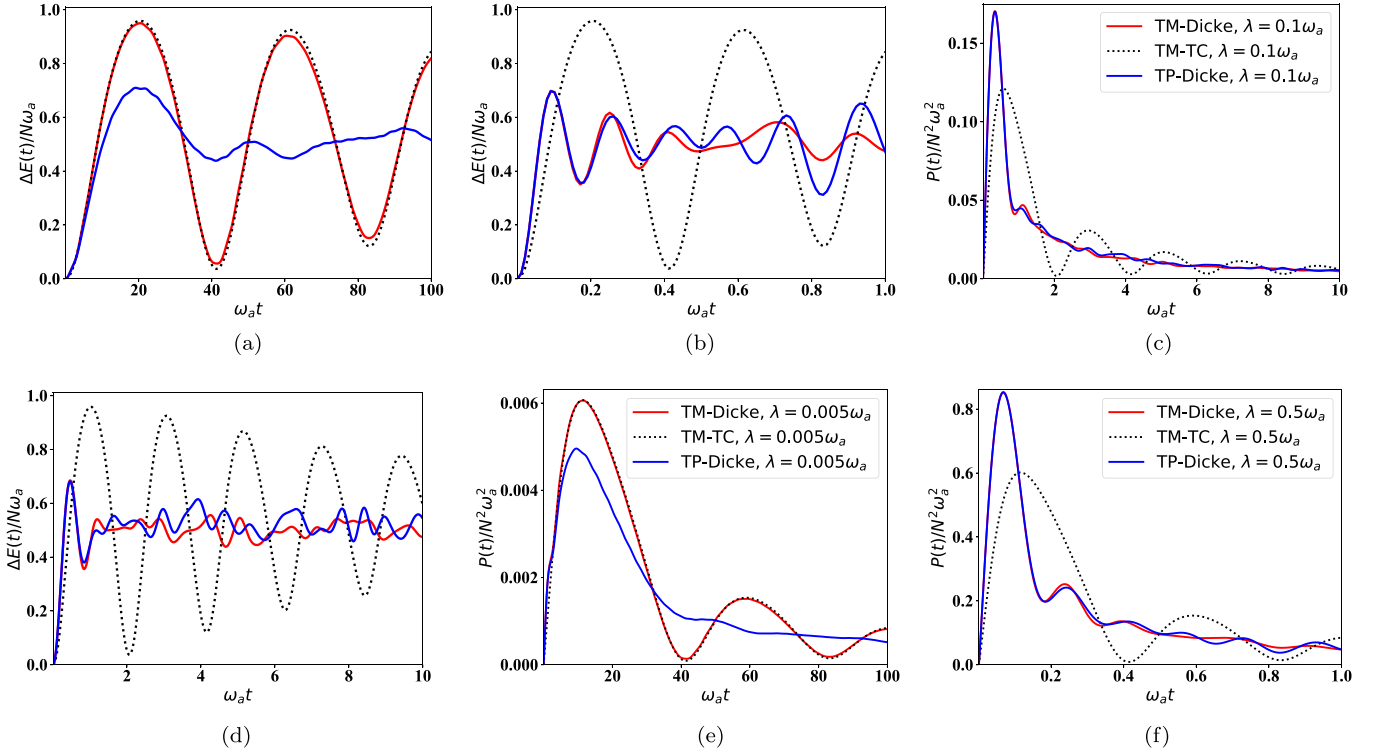


FIG. 11. Evolution of energy $\Delta E(t)$ and average power $P(t)$ with time for the TM-Dicke QB (red solid line), the two-mode TC QB (black dashed line), and the TP-Dicke QB (blue solid line) at (a) and (d) $\lambda = 0.005\omega_a$, (b) and (e) $\lambda = 0.1\omega_a$, and (c) and (f) $\lambda = 0.5\omega_a$.

$P(t)$ for the two-mode Dicke model ($\lambda = 0.1\omega_a$) in comparison with the two-photon one and the two-mode TC model. The main result shows that the performances of the two-mode Dicke model and two-photon Dicke model are similar. It is worth noting that the maximum stored energy of the two-mode TC model ($\Delta E_{\max}^{(\text{TM-TC})}/N\omega_a \sim 0.959$) is much higher than those of the two-mode ($\Delta E_{\max}^{(\text{TM-Dicke})}/N\omega_a \sim 0.685$) and two-photon ($\Delta E_{\max}^{(\text{TP-Dicke})}/N\omega_a \sim 0.681$) cases. We can see that the absence of counterrotating terms can lead to a higher stored energy in the USC regime.

We now consider the average charging power $P(t)$ as reported in Fig. 11(e). The maxima of the charging power and the corresponding time are better in the two-mode Dicke and two-photon Dicke models ($P_{\max}^{[\text{TM}(\text{TP})\text{-Dicke}]} / N^2\omega_a^2 \sim 0.170$) compared to the two-mode TC case ($P_{\max}^{(\text{TM-TC})} / N^2\omega_a^2 \sim 0.121$). It obvious that the counterrotating terms can lead to a greater average charging power with respect to the TC model. That is to say, the counterrotating terms have a negative impact on the stored energy but improve the average charging power in the USC regime. Furthermore, the case with $\lambda = 0.5\omega_a$ is also studied; we obtain similar results and observe an improved charging power for higher coupling [see Figs. 11(c) and 11(f)].

VI. CONCLUSIONS

We investigated the performance of a series of two-mode QBs in this paper. Considering the possible initial states of a quantum radiation cavity, we studied three different scenarios, with the initial state of the two-mode cavity in the F-F state, in the F-C state, and in the C-C state. According to

the analysis, the initial state of the two-mode cavity in the F-F state is the ideal candidate initial state for optimizing the performance of the QB. It is the only state that can achieve full charging of the QB in a short time, and all the energy stored in it can also be extracted. In addition, we investigated the competitive relationship between entanglement and ergotropy analytically, presented the relationship between the ergotropy and battery-charger entanglement of the incoherent QB, and defined the resource utilization efficiency $k(t)$ and $k^{\text{ins}}(t)$. We showed that the entanglement can be seen as a key resource in the energy-extraction stage. We also provided a quantitative relationship between them. Interesting properties can also be found by studying the two cases with the two-mode cavity in the F-C state and in the C-C state with the same average number of photons.

Furthermore, we also investigated some derived QBs of the above model. Our results show that all four models can reach a fully charged state and at the moment t_E the energy fluctuation is zero. We observed that the charging time of the two-mode Raman QB is shorter and the efficiency is higher than that of the two-mode QB. Moreover, the model related to coupling strength can also improve the performance of batteries, including faster charging speed and higher efficiency. Among the derived models we have investigated, the two-mode Raman QB dependent on coupling strength showed the best performance. In addition, in the last section, we extended the above model to multiple TLSs and a cavity with counterrotating terms. We showed that counterrotating terms can improve the stored energy in the USC regime. Our analysis can also be extended to three-level systems. Since the two-mode QB can be realized in experiment, we believe that

our research will have a positive effect on promoting future study.

ACKNOWLEDGMENTS

This work was supported by the National Natural Science Foundation of China (Grant No. 12175179), the Peng Huanwu Center for Fundamental Theory (Grant No. 12247103), and the Natural Science Basic Research Program of Shaanxi Province (Grants No. 2021JCW-19 and No. 2019JQ-863).

APPENDIX A

In this Appendix, we derive the Hamiltonian which describes the more general nonlinear JC model. For this reason, we suppose the electric field $E(r, t)$ can be expanded in terms of normal modes,

$$\begin{aligned} E(r, t) &= i \sum_k \hat{e}_k \sqrt{\frac{\omega_k}{k}} [\hat{a}_k(t) U_k(r) - \hat{a}_k^\dagger(t) U_k(r)] \\ &= \sum_k \hat{e}_k [E_k^{(-)}(r, t) + E_k^{(+)}(r, t)]. \end{aligned} \quad (\text{A1})$$

The term $E_k^{(+)}(r, t)$ represents a signal mode of the electromagnetic field with frequency ω_k (in a cavity, say), while the operators \hat{a}_k (\hat{a}_k^\dagger) are the annihilation (creation) operators of the k th mode which satisfy the commutation relations given by

$$[\hat{a}_k, \hat{a}_{k'}^\dagger] = \delta_{kk'}, [\hat{a}_k, \hat{a}_{k'}] = 0. \quad (\text{A2})$$

The mode functions $U_k(r)$ are taken to satisfy the wave equation

$$(\nabla^2 + \omega_k^2) U_k(r) = 0, \quad (\text{A3})$$

with the orthonormality condition

$$\int d^3r U_k(r) U_{k'}(r) = \delta_{kk'}. \quad (\text{A4})$$

Therefore, the Hamiltonian describing the field \hat{H}_f can be written in the form

$$\hat{H}_f = \sum_k \omega_k \left(\hat{a}_k^\dagger \hat{a}_k + \frac{1}{2} \right). \quad (\text{A5})$$

Next, we write the expression for the interaction Hamiltonian \hat{H}_{in} which represents the interaction between the atom and the field. A general interaction Hamiltonian describing an $(m +$

$n)$ -photon process may be written as

$$\hat{H}_{in} = \varepsilon_{\alpha\beta}^{(n+m)} \hat{C}_\beta^\dagger \hat{C}_\alpha \prod_{j=1}^m E_j^{(-)}(r_0) \prod_{k=1}^n E_k^{(+)}(r_0) + \text{H.c.}, \quad (\text{A6})$$

where $\varepsilon_{\alpha\beta}^{(n+m)}$ is the matrix element for an $(n + m)$ -photon transition consisting of m emissions and n absorptions and an atomic transition from state α to state β of an atom situated at position r_0 occurs, while \hat{C}_β^\dagger (\hat{C}_β) represents the creation (annihilation) operator for atomic state β (Fermion operators).

Thus, \hat{H}_{in} can be written in the form

$$\hat{H}_{in} \sim \mu_{\alpha\beta}^{(n+m)} \hat{C}_\beta^\dagger \hat{C}_\alpha \prod_{j=1}^m \hat{a}_j \prod_{k=1}^n \hat{a}_k^\dagger + \text{H.c.}, \quad (\text{A7})$$

where the coupling constant $\mu_{\alpha\beta}^{(n+m)}$ stands for the expression

$$\begin{aligned} \mu_{\alpha\beta}^{(n+m)} &= \varepsilon_{\alpha\beta}^{(n+m)} \left(\prod_{j=1}^{m+n} i \sqrt{\frac{1}{2} \omega_j} \right) \left(\prod_{j=1}^n U_j(r_0) \right) \\ &\quad \times \left(\prod_{k=1}^m U_k^*(r_0) \right). \end{aligned} \quad (\text{A8})$$

The Hamiltonian representing the atom \hat{H}_A is given by

$$\hat{H}_A = \sum_{i=1}^2 \Omega_i \hat{C}_i^\dagger \hat{C}_i. \quad (\text{A9})$$

Thus, if we use the Schwinger representation,

$$\begin{aligned} \hat{\sigma}_+ &= \hat{C}_1^\dagger \hat{C}_2, \quad \hat{\sigma}_- = \hat{C}_2^\dagger \hat{C}_1, \quad \hat{\sigma}_z = \hat{C}_1^\dagger \hat{C}_1 - \hat{C}_2^\dagger \hat{C}_2, \\ \hat{I} &= \hat{C}_1^\dagger \hat{C}_1 = \hat{C}_2^\dagger \hat{C}_2, \end{aligned} \quad (\text{A10})$$

and take $\omega_0 = \Omega_1 - \Omega_2$ and a linear combination of Eqs. (A5), (A7), and (A9) under the restriction of two modes, we have, except for an energy shift, Eq. (2).

Adding two terms related to coupling strength to Eq. (2) changes the equation to Eq. (32). The coupling strength terms have many forms, and the previously recognized forms are

$$\hat{R}_- = \sqrt{\hat{a}^\dagger \hat{a}} \hat{a}^\dagger \hat{b}^\dagger \sqrt{\hat{b}^\dagger \hat{b}} \hat{\sigma}_-, \quad \hat{R}_+ = \sqrt{\hat{b}^\dagger \hat{b}} \hat{b} \hat{a} \sqrt{\hat{a}^\dagger \hat{a}} \hat{\sigma}_+, \quad (\text{A11})$$

where $N = \hat{a}^\dagger \hat{a}$ and $M = \hat{b}^\dagger \hat{b}$. In order to compare the performance of the two-mode QB and previous research results, we choose this special form and write the Hamiltonian of the two-mode QB dependent on coupling strength as Eq. (32).

APPENDIX B

The state function and the reduced density matrix of the TLS from calculating the partial trace of the cavity part at any time can be expressed as follows:

$$\begin{aligned} |\psi(t)\rangle &= e^{-i\hat{H}t} |\psi(0)\rangle = \sum_{n,m} \alpha_n \alpha_m e^{-i\frac{\omega_a}{2}(n+m-1)t} \left(\frac{e^{+i\lambda\sqrt{nm}t} |\psi_-^{(n,m)}\rangle + e^{-i\lambda\sqrt{nm}t} |\psi_+^{(n,m)}\rangle}{\sqrt{2}} \right) \\ &= \sum_{n,m} \alpha_n \alpha_m e^{-i\frac{\omega_a}{2}(n+m-1)t} \left(\frac{e^{+i\lambda\sqrt{nm}t} (|g, n, m\rangle - |e, n-1, m-1\rangle) + e^{-i\lambda\sqrt{nm}t} (|g, n, m\rangle + |e, n-1, m-1\rangle)}{2} \right) \\ &= \sum_{n,m} \alpha_n \alpha_m e^{-i\frac{\omega_a}{2}(n+m-1)t} [\cos(\lambda\sqrt{nm}t) |g, n, m\rangle - i \sin(\lambda\sqrt{nm}t) |e, n-1, m-1\rangle], \end{aligned} \quad (\text{B1})$$

$$\begin{aligned} \rho_{\text{TLS}}(t) &= \sum_{n,m} \langle n, m | \rho(t) | n, m \rangle = \sum_{n,m} ([P_n P_m \sin^2(\lambda\sqrt{mnt}) |e\rangle \langle e| + P_n P_m \cos^2(\lambda\sqrt{mnt}) |g\rangle \langle g|] \\ &+ e^{i\omega_a t} \{i\sqrt{P_n P_m P_{n+1} P_{m+1}} \sin[\lambda\sqrt{(n+1)(m+1)t}] \cos(\lambda\sqrt{mnt})\} |g\rangle \langle e| \\ &- e^{-i\omega_a t} \{i\sqrt{P_n P_m P_{n+1} P_{m+1}} \sin[\lambda\sqrt{(n+1)(m+1)t}] \cos(\lambda\sqrt{mnt})\} |e\rangle \langle g|). \end{aligned} \quad (\text{B2})$$

In the following, we will introduce the state function and the reduced density matrix of the TLS when the two-mode cavity is in the F-F state, F-C state, and C-C state at time t . For the case of the two-mode cavity in the F-F state, the state function and the density matrix of the whole system at time t are

$$|\psi^{\text{F-F}}(t)\rangle = e^{-i(n+m-1)\omega_c t} \cos(\lambda\sqrt{mnt}) |g, m, n\rangle - e^{-i(n+m-1)\omega_c t} i \sin(\lambda\sqrt{mnt}) |e, n-1, m-1\rangle, \quad (\text{B3})$$

$$\rho_{\text{TLS}}^{\text{F-F}}(t) = \text{Tr}_C[\rho(t)] = \text{Tr}_C[|\psi(t)\rangle \langle \psi(t)|] = \cos^2(\lambda\sqrt{mnt}) |g\rangle \langle g| + \sin^2(\lambda\sqrt{mnt}) |e\rangle \langle e|. \quad (\text{B4})$$

For the case of the two-mode cavity in the F-C state, the state function and the density matrix of the whole system at time t are

$$|\psi^{\text{F-C}}(t)\rangle = a_n e^{-i(n+m-1)\omega_c t} \cos(\lambda\sqrt{mnt}) |g, n, m\rangle - a_{n+1} e^{-i(n+m+1)\omega_c t} i \sin[\lambda\sqrt{(n+1)(m+1)t}] |e, n, m\rangle, \quad (\text{B5})$$

$$\begin{aligned} \rho_{\text{TLS}}^{\text{F-C}}(t) &= \text{Tr}_C[\rho(t)] = \text{Tr}_C[|\psi(t)\rangle \langle \psi(t)|] = \sum_n |a_{n+1}|^2 \sin^2[\lambda\sqrt{(n+1)(m+1)t}] |e\rangle \langle e| \\ &+ \sum_n -ia_n^* a_{n+1} e^{-i\omega_c t} \cos(\lambda\sqrt{mnt}) \sin[\lambda\sqrt{(n+1)(m+1)t}] |e\rangle \langle g| \\ &+ \sum_n ia_n a_{n+1}^* e^{i\omega_c t} \cos(\lambda\sqrt{mnt}) \sin[\lambda\sqrt{(n+1)(m+1)t}] |g\rangle \langle e| + \sum_n |a_n|^2 \cos^2(\lambda\sqrt{mnt}) |g\rangle \langle g|. \end{aligned} \quad (\text{B6})$$

For the case of the two-mode cavity in the C-C state, the state function and density matrix of the whole system at time t are

$$|\psi^{\text{C-C}}(t)\rangle = a_n a_m e^{-i(n+m-1)\omega_c t} \cos(\lambda\sqrt{mnt}) |g, n, m\rangle - a_{n+1} a_{m+1} e^{-i(n+m+1)\omega_c t} i \sin[\lambda\sqrt{(n+1)(m+1)t}] |e, n, m\rangle, \quad (\text{B7})$$

$$\begin{aligned} \rho_{\text{TLS}}^{\text{C-C}}(t) &= \text{Tr}_C[\rho(t)] = \text{Tr}_C[|\psi(t)\rangle \langle \psi(t)|] = \sum_{n,m} |a_{n+1}|^2 |a_{m+1}|^2 \sin^2[\lambda\sqrt{(n+1)(m+1)t}] |e\rangle \langle e| \\ &+ \sum_{n,m} -ia_n^* a_m^* a_{n+1} a_{m+1} e^{-i\omega_c t} \cos(\lambda\sqrt{mnt}) \sin[\lambda\sqrt{(n+1)(m+1)t}] |e\rangle \langle g| \\ &+ \sum_{n,m} ia_n a_m a_{n+1}^* a_{m+1}^* e^{i\omega_c t} \cos(\lambda\sqrt{mnt}) \sin[\lambda\sqrt{(n+1)(m+1)t}] |g\rangle \langle e| + \sum_{n,m} |a_n|^2 |a_m|^2 \cos^2(\lambda\sqrt{mnt}) |g\rangle \langle g|. \end{aligned} \quad (\text{B8})$$

-
- [1] Q. Zhang, F. H. Xu, L. Li, N.L. Liu, and J.W. Pan, Quantum information research in China, *Quantum Sci. Technol.* **4**, 040503 (2019).
- [2] M. G. Raymer and C. Monroe, The US national quantum initiative, *Quantum Sci. Technol.* **4**, 020504 (2019).
- [3] B. Sussman, P. Corkum, A. Blais, D. Cory, and A. Damascelli, Quantum Canada, *Quantum Sci. Technol.* **4**, 020503 (2019).
- [4] D. P. Di Vincenzo, Quantum computation, *Science* **270**, 255 (1995).
- [5] R. Alicki and M. Fannes, Entanglement boost for extractable work from ensembles of quantum batteries, *Phys. Rev. E* **87**, 042123 (2013).
- [6] J. Y. Gyhm, D. Šafránek, and D. Rosa, Quantum charging advantage cannot be extensive without global operations, *Phys. Rev. Lett.* **128**, 140501 (2022).
- [7] K. V. Hovhannissyan, M. Perarnau-Llobet, M. Huber, and A. Acín, Entanglement generation is not necessary for optimal work extraction, *Phys. Rev. Lett.* **111**, 240401 (2013).
- [8] D. Ferraro, M. Campisi, G. M. Andolina, V. Pellegrini, and M. Polini, High-power collective charging of a solid-state quantum battery, *Phys. Rev. Lett.* **120**, 117702 (2018).
- [9] F. H. Kamin, F. T. Tabesh, S. Salimi, and A. C. Santos, Entanglement, coherence, and charging process of quantum batteries, *Phys. Rev. E* **102**, 052109 (2020).
- [10] J. X. Liu, H. L. Shi, Y. H. Shi, X. H. Wang, and W. L. Yang, Entanglement and work extraction in the central-spin quantum battery, *Phys. Rev. B* **104**, 245418 (2021).
- [11] H. L. Shi, S. Ding, Q. K. Wan, X. H. Wang, and W. L. Yang, Entanglement, coherence, and extractable work in quantum batteries, *Phys. Rev. Lett.* **129**, 130602 (2022).
- [12] J. I. Cirac and P. Zoller, Quantum computations with cold trapped ions, *Phys. Rev. Lett.* **74**, 4091 (1995).
- [13] C. D. Bruzewicz, J. Chiaverini, R. McConnell, and J. M. Sage, Trapped-ion quantum computing: Progress and challenges, *Appl. Phys. Rev.* **6**, 021314 (2019).
- [14] I. Georgescu, Trapped ion quantum computing turns 25, *Nat. Rev. Phys.* **2**, 278 (2020).

- [15] M. H. Devoret and R. J. Schoelkopf, Superconducting circuits for quantum information: An outlook, *Science* **339**, 1169 (2013).
- [16] A. Singha, M. Gibertini, B. Karmakar, S. Yuan, M. Polini, G. Vignale, M. I. Katsnelson, A. Pinczuk, L. N. Pfeiffer, K. W. West, and V. Pellegrini, Two-dimensional Mott-Hubbard electrons in an artificial honeycomb lattice, *Science* **332**, 1176 (2011).
- [17] Y. Y. Zhang, T. R. Yang, L. Fu, and X. Wang, Powerful harmonic charging in a quantum battery, *Phys. Rev. E* **99**, 052106 (2019).
- [18] F. Q. Dou, Y. Q. Lu, Y. J. Wang, and J. A. Sun, Extended Dicke quantum battery with interatomic interactions and driving field, *Phys. Rev. B* **105**, 115405 (2022).
- [19] S. Haroche and J. M. Raimond, *Exploring the Quantum: Atoms, Cavities, and Photons* (Oxford University Press, Oxford, 2006).
- [20] R. J. Schoelkopf and S. M. Girvin, Wiring up quantum systems, *Nature (London)* **451**, 664 (2008).
- [21] T. P. Le, J. Levinsen, K. Modi, M. M. Parish, and F. A. Pollock, Spin-chain model of a many-body quantum battery, *Phys. Rev. A* **97**, 022106 (2018).
- [22] G. M. Andolina, M. Keck, A. Mari, M. Campisi, V. Giovannetti, and M. Polini, Extractable work, the role of correlations, and asymptotic freedom in quantum batteries, *Phys. Rev. Lett.* **122**, 047702 (2019).
- [23] D. Rossini, G. M. Andolina, D. Rosa, M. Carrega, and M. Polini, Quantum advantage in the charging process of Sachdev-Ye-Kitaev batteries, *Phys. Rev. Lett.* **125**, 236402 (2020).
- [24] G. M. Andolina, M. Keck, A. Mari, V. Giovannetti, and M. Polini, Quantum versus classical many-body batteries, *Phys. Rev. B* **99**, 205437 (2019).
- [25] W. Lu, J. Chen, L. M. Kuang, and X. Wang, Optimal state for a Tavis-Cummings quantum battery via the Bethe ansatz method, *Phys. Rev. A* **104**, 043706 (2021).
- [26] F. C. Binder, S. Vinjanampathy, K. Modi, and J. Goold, QuantaCell: Powerful charging of quantum batteries, *New J. Phys.* **17**, 075015 (2015).
- [27] L. W. Duan, Y. F. Xie, D. Braak, and Q. H. Chen, Two-photon Rabi model: Analytic solutions and spectral collapse, *J. Phys. A* **49**, 464002 (2016).
- [28] L. W. Duan, S. He, D. Braak, and Q. H. Chen, Solution of the two-mode quantum Rabi model using extended squeezed states, *Europhys. Lett.* **112**, 34003 (2015).
- [29] S. Singh and K. Gilhare, Dynamics for a two-atom two-mode intensity-dependent Raman coupled model, *J. Exp. Theor. Phys.* **122**, 984 (2016).
- [30] S. Singh and A. Sinha, Solutions of two-mode Jaynes-Cummings models, *Pramana* **70**, 887 (2008).
- [31] Y. F. Gao, J. Feng, and J. S. Wang, Evolution of field entropy and entanglement in the intensity-dependent two-mode Jaynes-Cummings model, *Chin. Phys.* **14**, 980 (2005).
- [32] A. Crescente, M. Carrega, M. Sassetti, and D. Ferraro, Ultrafast charging in a two-photon Dicke quantum battery, *Phys. Rev. B* **102**, 245407 (2020).
- [33] A. Delmonte, A. Crescente, M. Carrega, D. Ferraro, and S. Sassetti, Characterization of a two-photon quantum battery: Initial conditions, stability and work extraction, *Entropy* **23**, 612 (2021).
- [34] G. M. Andolina, D. Farina, A. Mari, V. Pellegrini, V. Giovannetti, and M. Polini, Charger-mediated energy transfer in exactly solvable models for quantum batteries, *Phys. Rev. B* **98**, 205423 (2018).
- [35] F. Mazzoncini, V. Cavina, G. M. Andolina, P. A. Erdman, and V. Giovannetti, Optimal control methods for quantum batteries, *Phys. Rev. A* **107**, 032218 (2023).
- [36] A. Crescente, M. Carrega, M. Sassetti, and D. Ferraro, Charging and energy fluctuations of a driven quantum battery, *New J. Phys.* **22**, 063057 (2020).
- [37] F. Caravelli, G. Coulter-DeWit, L. P. García-Pintos, and A. Hamma, Random quantum batteries, *Phys. Rev. Res.* **2**, 023095 (2020).
- [38] N. Friis and M. Huber, Precision and work fluctuations in Gaussian battery charging, *Quantum* **2**, 61 (2018).
- [39] S. Imai, O. Gühne, and S. Nimmrichter, Work fluctuations and entanglement in quantum batteries, *Phys. Rev. A* **107**, 022215 (2023).
- [40] A. E. Allahverdyan, R. Balian, and T. M. Nieuwenhuizen, Maximal work extraction from finite quantum systems, *Europhys. Lett.* **67**, 565 (2004).
- [41] G. Francica, F. C. Binder, G. Guarnieri, M. T. Mitchison, J. Goold, and F. Plastina, Quantum coherence and ergotropy, *Phys. Rev. Lett.* **125**, 180603 (2020).
- [42] A. C. Santos, Quantum advantage of two-level batteries in the self-discharging process, *Phys. Rev. E* **103**, 042118 (2021).
- [43] P. Strasberg, G. Schaller, T. Brandes, and M. Esposito, Quantum and information thermodynamics: A unifying framework based on repeated interactions, *Phys. Rev. X* **7**, 021003 (2017).
- [44] F. Campaioli, F. A. Pollock, F. C. Binder, L. Céleri, J. Goold, S. Vinjanampathy, and K. Modi, Enhancing the charging power of quantum batteries, *Phys. Rev. Lett.* **118**, 150601 (2017).
- [45] J. M. Fink, R. Bianchetti, M. Baur, M. Göppl, L. Steffen, S. Filipp, P. J. Leek, A. Blais, and A. Wallraff, Dressed collective qubit states and the Tavis-Cummings model in circuit QED, *Phys. Rev. Lett.* **103**, 083601 (2009).
- [46] B. Buck and C. V. Sukumar, Exactly soluble model of atom-phonon coupling showing periodic decay and revival, *Phys. Lett. A* **81**, 132 (1981).
- [47] M. S. Abdalla, M. M. A. Ahmed, and A.-S. F. Obada, Multimode and multiphoton processes in a non-linear Jaynes-Cummings model, *Physica A* **170**, 393 (1991).
- [48] R. H. Dicke, Coherence in spontaneous radiation processes, *Phys. Rev.* **93**, 99 (1954).
- [49] A. Morales, D. Dreon, X. L. Li, A. Baumgärtner, P. Zupancic, T. Donner, and T. Esslinger, Two-mode Dicke model from nondegenerate polarization modes, *Phys. Rev. A* **100**, 013816 (2019).
- [50] R. R. Soldati, M. T. Mitchison, and G. T. Landi, Multipartite quantum correlations in a two-mode Dicke model, *Phys. Rev. A* **104**, 052423 (2021).
- [51] T. Niemczyk, F. Deppe, H. Huebl, E. P. Menzel, F. Hocke, M. J. Schwarz, J. J. Garcia-Ripoll, D. Zueco, T. Hümmer, E. Solano, A. Marx, and R. Gross, Circuit quantum electrodynamics in the ultrastrong-coupling regime, *Nat. Phys.* **6**, 772 (2010).
- [52] A. F. Kockum, A. Miranowicz, S. De Liberato, S. Savasta, and F. Nori, Circuit quantum electrodynamics in the ultrastrong-coupling regime, *Nat. Rev. Phys.* **1**, 19 (2019).